Acta Crystallographica Section F
Structural Biology and Crystallization Communications
ISSN 1744-3091

Crystallization and preliminary X-ray diffraction analysis of red clover necrotic mosaic virus

Stanton L. Martin,[a] Richard H. Guenther,[a] Tim L. Sit,[a] Paul D. Swartz,[b] Flora Meilleur,[b,c] Steven A. Lommel[a] and Robert B. Rose[b]*

[a]Department of Plant Pathology, North Carolina State University, Raleigh, North Carolina, USA, [b]Department of Molecular and Structural Biochemistry, North Carolina State University, Raleigh, North Carolina, USA, and [c]Oak Ridge National Laboratory, Oak Ridge, Tennessee, USA

Correspondence e-mail: bob_rose@ncsu.edu

Received 8 June 2010
Accepted 12 August 2010

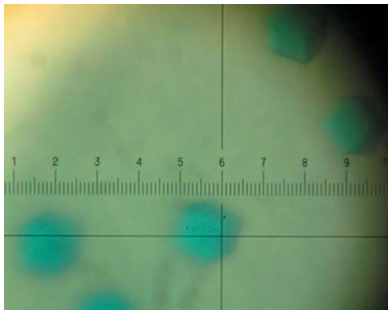

Red clover necrotic mosaic virus (RCNMV) is a species that belongs to the *Tombusviridae* family of plant viruses with a $T = 3$ icosahedral capsid. RCNMV virions were purified and were crystallized for X-ray analysis using the hanging-drop vapor-diffusion method. Self-rotation functions and systematic absences identified the space group as $I23$, with two virions in the unit cell. The crystals diffracted to better than 4 Å resolution but were very radiation-sensitive, causing rapid decay of the high-resolution reflections. The data were processed to 6 Å in the analysis presented here.

1. Introduction

Red clover necrotic mosaic virus (RCNMV) was first reported in *Trifolium pretense* (red clover) in the former Czechoslovakia (Musil, 1969). RCNMV naturally occurs in Australia, Poland, Canada and New Zealand (Hollings & Stone, 1977) and is a species that belongs to the *Dianthovirus* genus and the *Tombusviridae* family (Fauquet *et al.*, 2005). *Tombusviridae* are small icosahedral viruses that possess positive-sense single-stranded RNA genomes. *Dianthoviruses* can be distinguished from other genera in the family as they are the only members that have bipartite genomes. The RCNMV virion population is composed of two distinct virion types: a major population consisting of virions with one copy each of RNA-1 and RNA-2 and a minor population of virions that contain multiple copies of RNA-2 alone. This observation implies that a novel RNA-packaging scheme exists for RCNMV (Basnayake *et al.*, 2006). RNA-1 is 3889 nucleotides in length and contains three open reading frames (ORFs) that encode 27, 57 and 37 kDa polypeptides (Xiong & Lommel, 1989). A −1 ribosomal frameshifting mechanism allows translation to continue through the p27 ORF into the p57 ORF in order to produce catalytic quantities of the 88 kDa viral polymerase (Xiong *et al.*, 1993). The 3′-proximal ORF encodes the 37 kDa capsid protein (CP), which is translated from a subgenomic RNA. RNA-2 encodes the 35 kDa movement protein (MP; Lommel *et al.*, 1988), which also functions as a suppressor of host RNA-silencing activity (Powers *et al.*, 2008). The origin of assembly is located within the MP ORF (Basnayake *et al.*, 2009). A small degradation product of RNA-1 with unknown function, SR1f, is also co-packaged into RCNMV virions (Iwakawa *et al.*, 2008).

The RCNMV virion consists of 180 identical CP subunits arranged as a $T = 3$ icosahedron with an outer diameter of 36 nm and possessing an inner cavity of ∼17 nm (Sherman *et al.*, 2006). RCNMV is morphologically similar to carnation mottle virus (CarMV) and tomato bushy stunt virus (TBSV), which are members of different genera within the *Tombusviridae*. Both the CarMV and the TBSV virions crystallized in space group $I23$. The structure of CarMV has been solved to 3.2 Å resolution by molecular replacement using the TBSV coordinates as a search model (Harrison *et al.*, 1978; Morgunova *et al.*, 1994; Olson *et al.*, 1983). A moderate-resolution 8 Å structure of RCNMV has been obtained by cryoelectron microscopic (cryoEM) reconstruction (Sherman *et al.*, 2006). Structural comparisons and density-map fittings illustrated significant structural similarity of RCNMV and TBSV (Sherman *et al.*, 2006).

The high-resolution crystal structure of RCNMV is of particular interest because of its unique packaging, self-assembly and cargo-carrying properties. The space constraints imposed by the small capsid size relative to the ~5.8 kb of RNA that must be packaged suggest a novel packaging mechanism. The RCNMV capsid has a unique property in that it can be reversibly transitioned from a 'closed' or native state to an 'open' state (with pores) without capsid dissolution by depletion of divalent metal cations (Sherman *et al.*, 2006). These attributes make RCNMV an ideal biomolecule for nanotechnological applications (Franzen & Lommel, 2009). Viral capsids can be engineered to display specific targeting peptides and recent work has demonstrated that the interior cavity can be loaded with small-molecule cargo (Loo *et al.*, 2008). These programmed virus-based nano-cargo vessels have taken up and released cargo in mammalian cells. Thus, RCNMV can serve as a cell-specific delivery vehicle for therapeutic agents (Franzen & Lommel, 2009). We initiated structural studies in order to further characterize the properties of the virus. Here, we report for the first time the crystallization and initial analysis of crystals of the RCNMV virion.

2. Materials and methods

2.1. Virus propagation

RCNMV was maintained in 4–6-week-old *Nicotiana clevelandii*. Infections were initiated by mechanical inoculation of T7-derived infectious RNA transcripts of full-length RNA-1 and RNA-2 (Xiong & Lommel, 1991). The infection was propagated by sap transmission of the infected tissue. The infected plants were maintained in a temperature-controlled glasshouse at 291 ± 2 K and harvested 7–10 d post-inoculation.

2.2. Virus purification

Virus purification was based on a previously published protocol for RCNMV (Sherman *et al.*, 2006). 200–250 g of RCNMV-infected leaves were combined with two volumes of 0.2 *M* sodium acetate pH 5.3 and 0.1%(*v*/*v*) β-mercaptoethanol and homogenized in a Waring Pro MegaMix blender. The homogenized tissue was filtered through Grade 50 Veratec all-cotton cheesecloth into a 2 l beaker and allowed to settle on ice for 15 min. The mixture was centrifuged at 7000 rev min^{-1} for 30 min at 277 K in Nalgene 250 ml polypropylene centrifuge bottles using a Sorvall GSA rotor in a Sorvall RC-5B refrigerated superspeed centrifuge. The supernatant was decanted through a sheet of 1R Miracloth (EMD Chemicals Inc., USA) into a 1 l beaker. A 1/4 volume of 40%(*w*/*v*) polyethylene glycol (PEG 8000) in 1 *M* NaCl solution was added to the supernatant and the solution was incubated on ice for 2 h. The solution was centrifuged again at 7000 rev min^{-1} for 30 min. The supernatant from each bottle was discarded and the pellets were resuspended in a 50 ml total volume of 0.2 *M* sodium acetate pH 5.3. The suspension was divided into two 25 ml aliquots in 30 ml Corex glass test tubes and centrifuged for 20 min at 10 000 rev min^{-1} in a Sorvall SS-34 rotor. The supernatant was aliquoted into six Beckman Ultra-Clear ultracentrifuge tubes (5 ml capacity), placed in a Beckman SW 55 Ti rotor and centrifuged at 48 000 rev min^{-1} for 90 min at 278 K. The supernatant was discarded and each pellet was resuspended by the addition of 200 µl 0.2 *M* sodium acetate pH 5.3 and incubation at 277 K overnight. The resuspended pellets were subsequently pooled. The virion concentration was determined by UV spectroscopy using a Nanodrop 1000 spectrophotometer (Thermo Scientific, Waltham, Massachusetts, USA) with an extinction coefficient of 6.46 mg ml^{-1} cm^{-1} and subsequently confirmed using the Coomassie Plus Protein Assay Reagent (Pierce Chemical, Rockford, Illinois, USA). A typical preparation yielded 70–100 µg of purified RCNMV per gram of infected tissue. The virus preparation was aliquoted into two 1.5 ml microfuge tubes and allowed to settle at 277 K for 21 d. During this time the sample separated into two fractions. The top fraction, which contained approximately half of the initial concentration, was used for subsequent crystallization experiments.

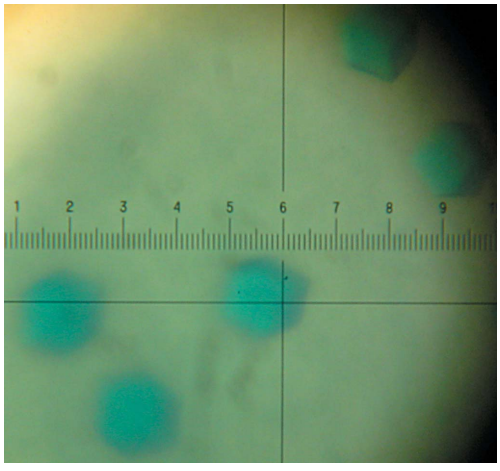

Figure 1
Crystals of RCNMV stained with Izit dye. Each minor tick in the scale represents 10 µm. The distance between numbered units is 100 µm.

2.3. Virus purity assays

Virion morphology and integrity were determined by transmission electron microscopy (TEM). Purified virus samples for TEM were diluted 1:10 000 by the addition of sodium acetate buffer. 5 µl of the diluted sample was placed on 400-mesh copper grids and negatively stained with 2%(*w*/*v*) uranyl acetate. The grids were examined using a JEM100S transmission electron microscope (Jeol, Peabody, Massachusetts, USA). The microscope was operated at 80 kV with magnification at 50 000×.

Dynamic light-scattering (DLS) data were collected using a Malvern 1000ES Zetasizer (Malvern Instruments, Worcestershire, England). Virus sample concentrations ranged from 15 to 30 mg ml^{-1}. DLS measurements were conducted at room temperature.

2.4. Crystallization

Initial crystallization trials utilized the sitting-drop vapor-diffusion technique at 291 K. Initial crystallization conditions tested included Crystal Screen, Crystal Screen 2, PEG/Ion, PEG/Ion 2 and Crystal Screen HT from Hampton Research (Aliso Viejo, California, USA), Structure Screens I and II from Molecular Dimensions Ltd (Apopka, Florida, USA) and Wizard I, II and III screens from Emerald BioSystems (Bainbridge Island, Washington, USA). 1 µl virion solution (15 mg ml^{-1}) was mixed with 1 µl crystallization solution and equilibrated against a 500 µl reservoir of crystallization solution. Crystals formed reliably with Molecular Dimensions Ltd Structure Screen I condition No. 10 (0.1 *M* trisodium citrate, 1.0 *M* ammonium dihydrogen phosphate pH 5.6) within 10 d. The crystals grown under this condition were stained with Izit crystal dye (Hampton Research) to confirm that they were not salt crystals. The dyed crystals are shown in Fig. 1. Crystals grew between pH 4.5 and 5.6; however, the optimal pH for crystallization was 4.7. The crystals were cube-shaped and had

Table 1
Data-collection statistics.

Values in parentheses are for the highest resolution shell.

Wavelength (Å)	1.00
Space group	*I*23
Unit-cell parameter (Å)	a = 377.8
No. of observations	70305
No. of unique reflections	21104
Multiplicity	3.3
Crystal mosaicity (°)	0.54
Resolution range (Å)	119–6.0 (6.33–6.0)
Completeness (%)	94.1 (96.0)
$R_{\rm merge}$ (%)	18.4 (40.3)
$\langle I/\sigma(I)\rangle$	2.8 (1.8)
Mean (I/sd)	4.8 (3.1)

a length of 75–100 µm. Crystals formed reliably under this condition utilizing both the sitting-drop and hanging-drop techniques. It was found that the crystals were easier to harvest when the hanging-drop technique was used, hence all crystals subsequent to the trial crystals were grown using the hanging-drop method. Three cryoprotectants were screened on our home RuH2R rotating-anode X-ray generator (Rigaku Corp., Tokyo, Japan) with a MAR 345 image-plate detector: 25% 2-methyl-2,4-pentanediol (MPD), 25% glycerol and 25% polyethylene glycol 400 (PEG 400). The PEG 400-treated crystals produced the highest resolution reflections with the least background.

2.5. Data collection and processing

Crystals were harvested with a nylon loop (Teng, 1990) and quickly dipped in cryoprotectant (a 1:1 mixture of crystallization solution and 25% PEG 400) prior to flash-cooling in liquid nitrogen. The data were collected on the SER-CAT beamline at the Advanced Photon Source, US Department of Energy Argonne National Laboratory (Argonne, Illinois, USA). The crystal-to-detector distance was set to 600 mm. An oscillation angle of 0.25° was used to minimize overlaps. Data were collected from a single crystal. The crystal initially diffracted to better than 4 Å resolution (Fig. 2). Data were processed using *MOSFLM* (Leslie, 1992) and scaled with *SCALA* from the *CCP*4 suite (Collaborative Computational Project, Number 4, 1994). The crystals were very radiation-sensitive, as indicated by a fivefold increase of the scaling factor within 100 frames (data not shown).

In order to determine the space group, the data were processed in space groups *P*23, *I*23, *P*3, *H*3 and *I*222. Self-rotation functions were generated using *POLARRFN* and visualized with the program *xplot*84*viewer* (Collaborative Computational Project, Number 4, 1994). The noncrystallographic symmetry and systematic absences indicated that the virion crystallized in space group *I*23, with unit-cell parameter a = 377.8 Å. Data statistics are presented in Table 1. The theoretical molecular weight of the virion based on the calculated mass of 180 CP subunits and the two genomic RNA molecules is ∼8.3 MDa. This yields a Matthews coefficient of 3.24 Å^3 Da^{-1} with two virions in the unit cell (Matthews, 1968). Using this method, the solvent content was calculated to be 62%. An alternative estimate was derived by estimating the volume of an icosohedron [$V = (5/12)(3 + 5^{1/2})a^3$, where a is the length of the edge]. This method yielded a solvent content of ∼51%.

3. Results and discussion

3.1. Sample characterization

Transmission electron micrographs indicated that the sample contained particles of uniform size and with highly similar morphology (Fig. 3). A small portion of the particles appeared to be misshapen, while others showed evidence of internal strain, suggesting some loss of capsid integrity. It was observed that samples that were allowed to settle for 21 d were better at forming crystals. After settling, the A_{260} absorbance was approximately half of the original value. Analysis of a settled sample found that the precipitated fraction had a slightly larger diameter as measured by DLS. This

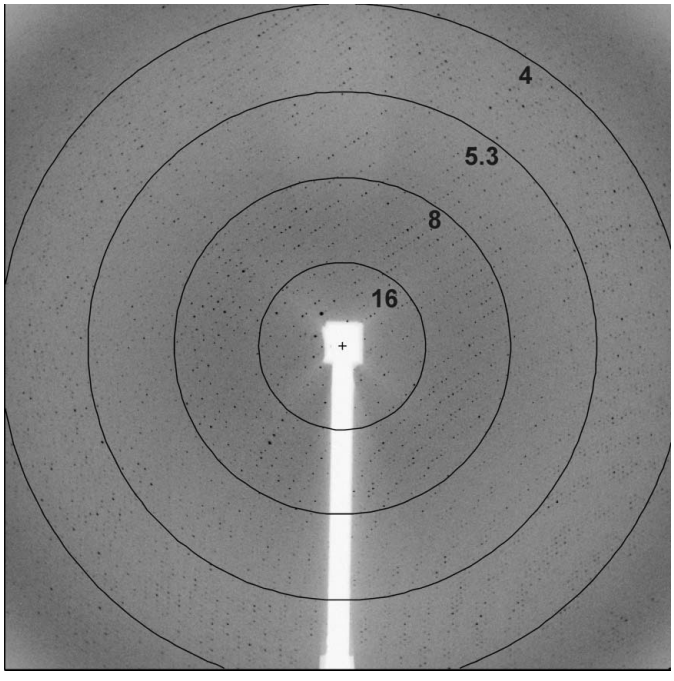

Figure 2
Diffraction of RCNMV crystals. The RCNMV crystals diffracted to 4 Å resolution. The first diffraction frame is displayed, with an oscillation angle of 0.25°. The resolution rings are at 16, 8, 5.3 and 4 Å resolution.

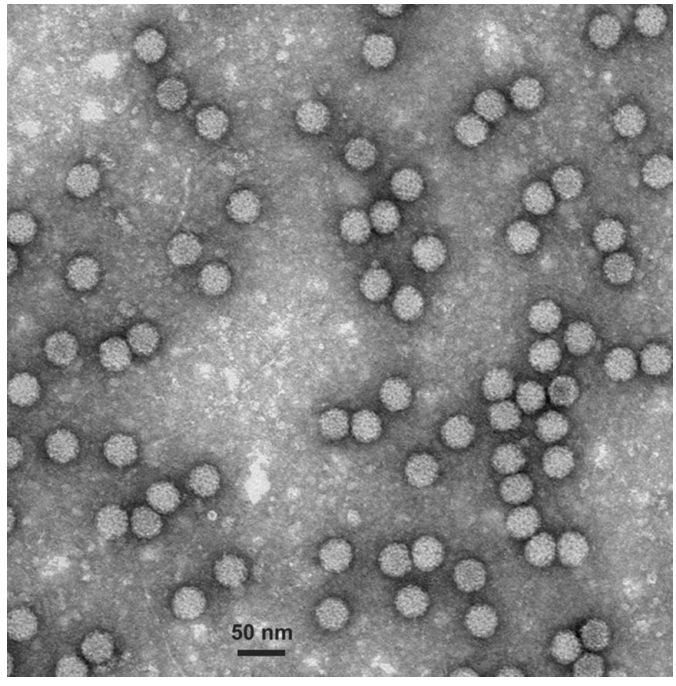

Figure 3
Transmission electron micrograph of RCNMV virions. Monodisperse intact viruses are shown at 50 000× magnification.

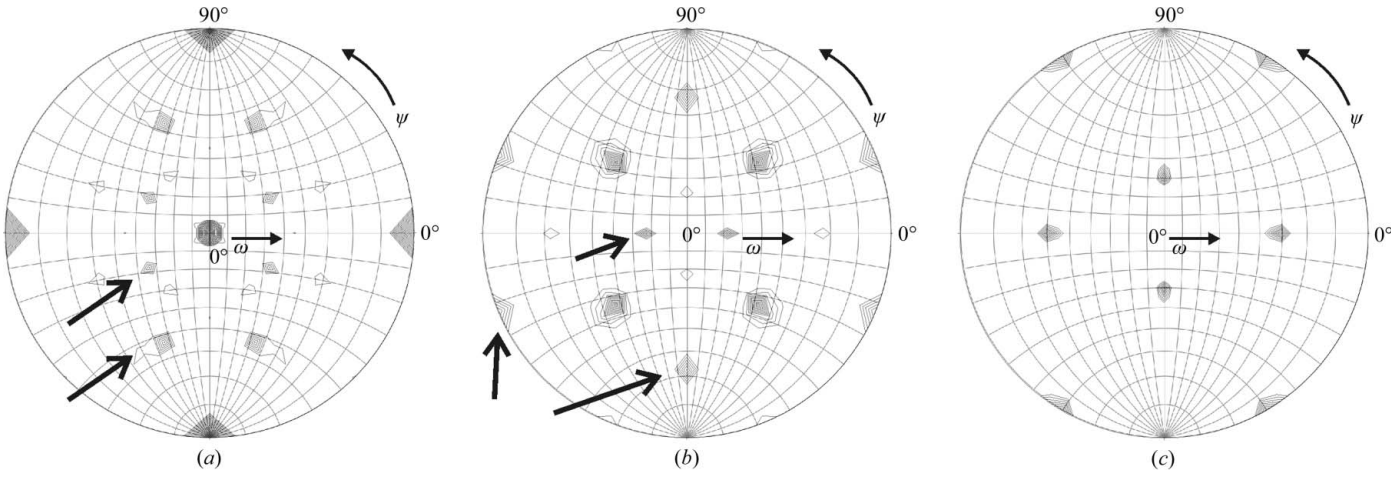

Figure 4
Self-rotation functions of the data reduced in *I*23 indicate noncrystallographic icosahedral symmetry of the virus. (*a*) Twofold symmetry axes, $\kappa = 180^\circ$. (*b*) Threefold symmetry axes, $\kappa = 120^\circ$. (*c*) Fivefold symmetry axes, $\kappa = 72^\circ$. In (*a*) and (*b*) arrows point to the noncrystallographic symmetry axes. All fivefold axes are noncrystallographic. The contour levels for (*a*) and (*b*) start at 10σ with a contour interval of 4σ. The contour levels for (*c*) start at 40σ with a contour interval of 8σ. The maximum integration radius for these plots was 120 Å using data in the 20–7 Å resolution range. Plots are drawn in polar coordinates.

step appears to selectively remove damaged or degraded particles. Virions which were not structurally intact precipitated, while the more stable intact population remained in solution.

3.2. RCNMV crystals

We have, for the first time to our knowledge, grown diffraction-quality crystals of RCNMV. The crystals diffracted to better than 4 Å resolution (Fig. 2). Owing to damage to the crystals upon prolonged exposure to synchrotron radiation, we were unable to collect a complete data set. Nevertheless, the data were of sufficient quality to identify the space group. The limited resolution of the data made it difficult to evaluate the space group from $R_{\rm merge}$ statistics alone. We therefore confirmed the space group through self-rotation functions. If the data were reduced in *I*23, the self-rotation functions included noncrystallographic twofold, threefold and fivefold operators of the virus (Fig. 4). This was not true if the data were reduced in *H*3 or *I*222 (not shown). Reducing the data in space group *P*23 confirmed the expected systematic absences in *I*23 (not shown).

The unit cell in space group *I*23 contains two virions per unit cell. The solvent content of the crystal is 62%, as calculated from the Matthews coefficient. This value is reasonable given the known dimension of the virion: 36 nm as measured by CryoEM (Sherman *et al.*, 2006). From the formula for the volume of an icosahedron, the solvent content would be 51% with two virions in the unit cell.

4. Conclusions

We present preliminary diffraction data and analysis demonstrating that the RCNMV crystals are of sufficient quality to ultimately determine the X-ray structure of the capsid at higher than 4 Å resolution. A data-collection strategy will be devised to minimize radiation exposure and may require the merging of multiple data sets to maximize the completeness of the data at high resolution. There is currently no crystal structure available of the RCNMV capsid, but there is a 7 Å resolution cryoEM structure (Sherman *et al.*, 2006). A 2.9 Å resolution structure exists for the structurally similar TBSV capsid (Olson *et al.*, 1983). The TBSV CP coordinates derived from the X-ray structure (Olson *et al.*, 1983) and the RCNMV CP co-ordinates derived by cryoEM (Sherman *et al.*, 2006) will be used to solve the crystal structure by molecular replacement. The overall identity and similarity between the RCNMV and TBSV CPs are 26% and 39%, respectively. The S domains are the most closely related (35% identical, 48% similar), while the P domains are 27% identical and 44% similar (Sherman *et al.*, 2006). The high-resolution structure of the virus will allow us to characterize and redesign the virion to optimize encapsidation, transport stability and targeted delivery.

We thank Carol George for host plant cultivation, Greg Burhman for technical advice and Professor Stefan Franzen for partial financial support. This work was funded in part by NSF Grant MCB-0651263. Data were collected at Southeast Regional Collaborative Access Team (SER-CAT) 22-ID beamline at the Advanced Photon Source, Argonne National Laboratory. Supporting institutions may be found at http://www.ser-cat.org/members.html. Use of the Advanced Photon Source was supported by the U. S. Department of Energy, Office of Science, Office of Basic Energy Sciences, under Contract No. W-31-109-Eng-38.

References

Basnayake, V. R., Sit, T. L. & Lommel, S. A. (2006). *Virology*, **345**, 532–539.
Basnayake, V. R., Sit, T. L. & Lommel, S. A. (2009). *Virology*, **384**, 169–178.
Collaborative Computational Project, Number 4 (1994). *Acta Cryst.* D**50**, 760–763.
Fauquet, C. M., May, M. A., Maniloff, J., Desselberger, U. & Ball, L. A. (2005). *Virus Taxonomy: VIIIth Report of the International Committee on Taxonomy of Viruses.* New York: Elsevier.
Franzen, S. & Lommel, S. A. (2009). *Nanomedicine*, **4**, 575–588.
Harrison, S. C., Olson, A. J., Schutt, C. E., Winkler, F. K. & Bricogne, G. (1978). *Nature (London)*, **276**, 368–373.
Hollings, M. & Stone, O. M. (1977). *CMI/AAB Descriptions of Plant Viruses*, No. 181. Warwick: Association of Applied Biologists. http://www.dpvweb.net/dpv/index.php.
Iwakawa, H. O., Mizumoto, H., Nagano, H., Imoto, Y., Takigawa, K., Sarawaneeyaruk, S., Kaido, M., Mise, K. & Okuno, T. (2008). *J. Virol.* **82**, 10162–10174.
Leslie, A. G. W. (1992). *Jnt CCP4/ESF–EACBM Newsl. Protein Crystallogr.* **26**.
Lommel, S. A., Weston-Fina, M., Xiong, Z. & Lomonossoff, G. P. (1988). *Nucleic Acids Res.* **16**, 8587–8602.
Loo, L., Guenther, R. H., Lommel, S. A. & Franzen, S. (2008). *Chem. Commun.*, pp. 88–90.
Matthews, B. W. (1968). *J. Mol. Biol.* **33**, 491–497.

Morgunova, E. Y., Dauter, Z., Fry, E., Stuart, D. I., Stel'mashchuk, V. Y., Mikhailov, A. M., Wilson, K. S. & Vainshtein, B. K. (1994). *FEBS Lett.* **338**, 267–271.
Musil, M. (1969). *Acta Virol.* **13**, 226–235.
Olson, A. J., Bricogne, G. & Harrison, S. C. (1983). *J. Mol. Biol.* **171**, 61–93.
Powers, J. G., Sit, T. L., Heinsohn, C., George, C. G., Kim, K.-H. & Lommel, S. A. (2008). *Virology*, **381**, 277–286.
Sherman, M. B., Guenther, R. H., Tama, F., Sit, T. L., Brooks, C. L., Mikhailov, A. M., Orlova, E. V., Baker, T. S. & Lommel, S. A. (2006). *J. Virol.* **80**, 10395–10406.
Teng, T.-Y. (1990). *J. Appl. Cryst.* **23**, 387–391.
Xiong, Z., Kim, K. H., Lendall, T. L. & Lommel, S. A. (1993). *Virology*, **193**, 213–221.
Xiong, Z. & Lommel, S. A. (1989). *Virology*, **171**, 543–554.
Xiong, Z. & Lommel, S. A. (1991). *Virology*, **182**, 388–392.